Electrochimica Acta 359 (2020) 136955

Contents lists available at ScienceDirect

Electrochimica Acta

journal homepage: www.elsevier.com/locate/electacta

$LiBO_2$-modified $LiCoO_2$ as an efficient cathode with garnet framework $Li_{6.75}La_3Zr_{1.75}Nb_{0.25}O_{12}$ electrolyte toward building all-solid-state lithium battery for high-temperature operation

Balasubramaniam Ramkumar[a], Kim So-young[a], Nam Chan-woo[a], Vanchiappan Aravindan[b], Lee Yun-Sung[a,*]

[a] Department of Advanced Chemicals and Engineering, Chonnam National University, Gwang-ju 61186, Republic of Korea
[b] Department of Chemistry, Indian Institute of Science Education and Research (IISER), Tirupati 517507, India

ARTICLE INFO

Article history:
Received 28 April 2020
Revised 13 August 2020
Accepted 13 August 2020
Available online 19 August 2020

Keywords:
LLZO solid electrolyte
LCO cathode
All solid-state Li-ion battery
$LiBO_2$ modification
Electrode/electrolyte interface

ABSTRACT

Garnet-based all-solid-state Li-ion batteries (ASSLIBs) suffer from high interfacial resistance at the cathode/electrolyte interface. Herein, we propose a $LiBO_2$ (LBO) modification over a $LiCoO_2$ (LCO) cathode to improve the interfacial contact and subsequently, the electrochemical performance of the cell. The High-Resolution Transmission Electron Microscopy (HR-TEM) images of the cathode particle show that the $LiBO_2$ (LBO) content on the LCO surface effectively improves the electrode/electrolyte interface. In the cut-off voltage range of 3 – 4.3 V *vs.* Li, the LBO-LCO maintains 50% of its initial capacity (60 mAh g^{-1}) after the 40th cycle, which is much higher than bare LCO in the ASSLIB configuration. The LBO layer over LCO enhances the Li-ion diffusion kinetics and eventually improves the electrochemical performance of the cell. To suppress the mechanical degradation of the electrode/electrolyte interface, we have reduced the working potential window to 3 – 4.1 V *vs.* Li, where the LBO-modified LCO provides an initial discharge capacity of 101 mAh g^{-1} and assists in realizing improved cyclic performance in comparison with the conventional potential window.

1. Introduction

The development of environment-friendly energy conversion and storage systems is essential to alleviate the challenges of ecological deterioration, the greenhouse effect, and the depletion of fossil fuels. In the last few decades, Li-ion batteries have been used in portable electronics and electric vehicles because of their high energy in both volumetric and gravimetric scale over other secondary batteries like Pb-acid, Ni-Cd, and Ni-MH. However, Li-ion batteries have major drawbacks, such as flammable solvents, limited power capability, and the formation of Li dendrites. Therefore, to improve safety, it has been proposed to replace the liquid counterpart with a solid electrolyte by retaining metallic Li as the anode [1,2]. Generally, the solid electrolyte or the fast Li-ion conductor is considered the heart of the all-solid-state Li-ion battery (ASSLIB) concept. For the complete realization of the ASSLIB configuration, the battery should operate at ambient or realistic temperatures, and the solid electrolytes should have high ionic conductivity ($>10^{-4}$ S cm^{-1}) with negligible electronic conductivity ($\sigma = 10^{-12}$ S cm^{-1}) and be capable of operating over a wide potential window (> 5 V *vs.* Li) [3]. The most commonly reported ceramic solid-electrolytes are perovskite ($Li_{3.3}La_{0.56}TiO_3$) [4,5], sodium superionic conductor (NASICON) ($LiTi_2(PO_4)_3$) [6], garnet-type $Li_7La_3Zr_2O_{12}$ [7,8] and LISICON ($Li_{14}Zn(GeO_4)_4$) [9], thio-LISCICON ($Li_{10}GeP_2S_{12}$) [10,11], anti-perovskite Li_3OX ($X = Cl^-$, Br^-, I^-) [12], and argyrodite Li_6PS_5X (X = Cl, Br, I) [13] structures.

Even though the NASICON and perovskite-based material show high ionic conductivity (10^{-4} S/cm > S cm^{-1}), their chemical instability (Ti^{4+} reduction) against the Li metal anode is worth mentioning [14,15]. In contrast, sulfide-based solid electrolytes have high ionic conductivity, excellent mechanical strength, and low grain boundary resistance, but they produce dangerous H_2S gas when they react with moisture; in addition, the poor compatibility of sulfide-based solid electrolytes with oxide cathode materials is an issue [16,17]. Compared with other ceramic electrolytes, the garnet $Li_{6.75}La_3Zr_{1.75\times0.25}(X$ = Nb, Ta)O_{12} solid electrolyte is considered a superior choice because of its excellent thermal stability, comparable ionic conductivity, and low reduction potential against the Li metal anode [14,18]. However, the high interfacial resistance at electrode-electrolyte interfaces is a longstanding problem associated with the fabrication of solid-state batteries. Therefore, it is

* Corresponding author.
E-mail address: leeys@chonnam.ac.kr (L. Yun-Sung).

https://doi.org/10.1016/j.electacta.2020.136955
0013-4686/

necessary to overcome interfacial issues to improve the electrochemical performance of these batteries. The space charge layer formation, structural disorder, and lattice mismatch are the main reasons for such high impedance across the interface in solid-state batteries [19,20]. The space charge layer formation in the interface is a result of the different Li chemical potentials in the electrode and electrolyte, which restrict the charge transfer rate. [21] Many attempts have been made to solve the above-mentioned issues, including metal oxide coating, phosphate coating, and carbonate formation on the surface of the cathode material; however, tackling the issue remains a challenge.

Buffer layer coating is an efficient technique that has many advantages, such as reducing the Li-deficient layer formation, the unwanted electrochemical reaction between the cathode and electrolyte, and cross-diffusion of elements. It has been suggested that $LiNbO_3$, $Li_4Ti_5O_{12}$, Li_4SiO_4-Li_3PO_4, and Li_4GeO_4-Li_3PO_4 modifications can significantly suppress the interfacial resistance when using a sulfide-based solid-state electrolyte [22,23,24]. Nevertheless, electrode and electrolyte attachment in an oxide electrolyte is difficult because it is more brittle than a sulfide system. Interestingly, a few research groups have improved the cathode/electrolyte interface by coating of $LiCoO_2$ (LCO) thin films on the electrolyte by magnetron sputtering, pulsed laser deposition, and the sol-gel method [25,26,27]. However, the production of large-scale solid-state batteries remains limited because of the low energy density, which is attributed to the low active mass loading and high cost of equipment. [28] Slurry casting and printing methods can be used, but the utilization of polymeric binders is limited because it connects only the surface-active materials to the electrolyte. [29] The alternative technique of sintering at a high temperature can improve the physical contact between the cathode and electrolyte, but the formation of an electrochemically inactive phase and the cross-diffusion of elements in the interface remain as issues. [30] To overcome these challenges and achieve good contact at the interface, the chemically stable Li-ion conductive binder has been used in ASSLIBs. Unfortunately, very few studies have been carried out by a few research groups using Li_3BO_3 as a sintering aid to enhance the adhesion between the cathode and electrolyte [31,32]. Nevertheless, the performance of ASSLIBs is still inadequate for practical use because of the partial contact between the cathode particles during the electrochemical process. Therefore, in the present work, we intended to modify the cathode surface using a Li-ion-based buffer layer coating ($LiBO_2$, LBO) to improve the electrochemical performance of LCO in the ASSLIB configuration. The main advantage of using LBO is its low melting point and high deformability. The coated LBO was melted at 700 °C for high-temperature treatment, forming a wide and homogeneous contact with the active material to increase its electrochemical utilization.

Herein, the bare LCO composite based ASSLIB displayed poor contact between the LCO and electrolyte; specifically, there is a gap between its interfaces. The poor contact in the cathode composite leads to high polarization for ion transfer and low discharge capacity during the electrochemical performance. The LBO modification over LCO particles was performed by the high-energy ball-milling method. The coated LBO provided good physical contact between the cathode and electrolyte and helped to decrease the resistance and fill the gap between the interfaces, which is highly favorable for facile Li-ion transfer. The LBO-coated LCO composite/garnet $Li_7La_3Zr_{1.75}Nb_{0.25}O_{12}$/Li metal in the ASSLIB cell affords a high discharge capacity and long cycling performance. The engineered interface improves the contact area and facilitates the Li-ion and electron transfer. The main objective of this work is to study the influence of buffer layer (LBO) coating on the LCO cathode active material in an ASSLIB. The galvanostatic charge/discharge performance of the cell confirms the high discharge capacity with good cycle life. We believe this work provides a new method to improve the cathode active material utilization and decrease the interfacial resistance of an oxide-based solid-state system.

2. Experimental section

2.1. Preparation of garnet solid-state batteries

The ASSLIB was constructed with an LCO cathode and Li metal anode separated by a $Li_{6.75}La_3Zr_{1.75}Nb_{0.25}O_{12}$ (LLZO) ceramic electrolyte. The LLZO solid electrolyte was prepared by the traditional solid-state method. Accordingly, the Li_2CO_3 (99%), La_2O_3 (99.9%), ZrO_2 (99%), and Nb_2O_5 (99.99%) precursors were dispersed in ethanol and ball-milled for 24 h in a high-energy ball-milling machine (Fritsch Pulverisette 6). Then, the resultant powder was dried at 60 °C and calcined at 950 °C for 18 h. The powder was again ball- milled for 24 h to improve the homogeneity and dried at 60 °C overnight. Then, the powder was pelletized by uniaxial pressing (10 MPa) and sintered at 1050 °C for 12 h (O_2 atmosphere) to prepare the LLZO solid electrolyte. The diameter and thickness of the pellet were estimated to be 1 cm and 1 mm, respectively.

The LBO (10 wt.%) was mixed with LCO particles (commercial powder) and ball-milled for 1 h in a high-energy ball-milling machine (Fig. 1). The LCO or LBO@LCO powder, LLZO solid electrolyte, and indium tin oxide (ITO) (weight ratio of 70:20:10) were mixed with ethyl cellulose binder and 1-methyl-2-pyrrolidone (NMP) solvent to prepare the cathode slurry. The indium tin oxide (ITO) is a new conductive material which has excellent stability and conductivity. [33] The obtained slurry was cast on the surface of the prepared solid electrolyte. After drying overnight, it was heated at 700 °C for 1 h to improve the interfacial contact. The actual mass loading of the active material was found to be 1 mg. The Li metal was attached to the opposite side of the pellet as an anode and liquefied for better anodic contact [Fig. 2]. A 2032-coin cell was assembled inside a glove box with a moisture content level of < 0.01 ppm. Before the electrochemical studies, the cell was heated to 80 °C to improve the interfacial contact across the electrode and electrolyte. For comparison, a prepared liquid cell consisted of LCO as the cathode and Li metal as the anode, separated by a polypropylene separator with 1 M $LiPF_6$ (EC: DMC for 1:1) as the electrolyte. The proportion of active material, ketjen black, and teflonized acetylene black (TAB-2) binder in the cathode electrode were 7:2:1. Before cell assembly, the attained mixtures were pressed on a stainless mesh current collector and dried in an oven at 160 °C for 4 h. Electrochemical studies were carried out between 3 and 4.3 V *vs.* Li at 25 °C.

2.2. Material characterization

Structural studies were performed using a powder X-ray diffractometer (XRD) with Cu Kα radiation (Rint 1000, Rigaku, Japan) in the range of 10–60° The surface morphology, cross-sectional image of the interface, and elemental composition were studied using a field-emission scanning electron microscope (FE-SEM, S-4700, Hitachi, Japan) coupled with an energy-dispersive X-ray spectroscopy (EDX) module. Pt was sputtered on both sides of the pellet by E-1030 ion sputter machine (Hitachi). The ionic conductivity of the LLZO pellet was calculated using a 4284A Precision LCR Meter between 1 MHz and 25 mHz with an applied amplitude of 1 mV. The a.c. impedance studies (EIS) and cyclic voltammetry (CV) of the solid-state battery were measured using an electrochemical analyzer (SP-150, Biologic, France). Electrochemical studies such as CV and galvanostatic charge-discharge studies were performed using an Arbin BT-2000 battery tester at 80 °C with various testing potential windows.

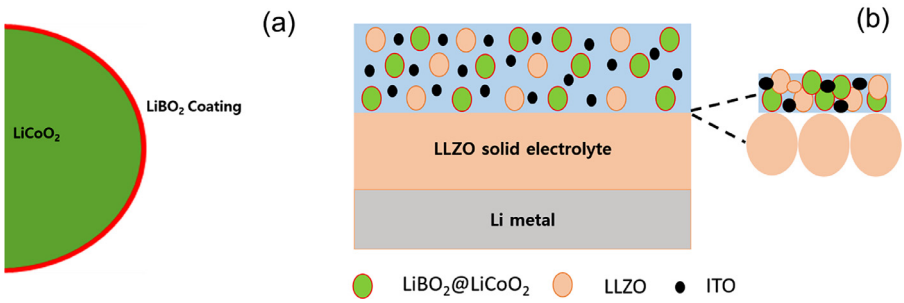

Fig. 1. (a) Schematic diagram for LBO coated on the surface of LCO particles, and (b) schematic diagram for LBO@LCO/LLZO/Li metal solid-state battery.

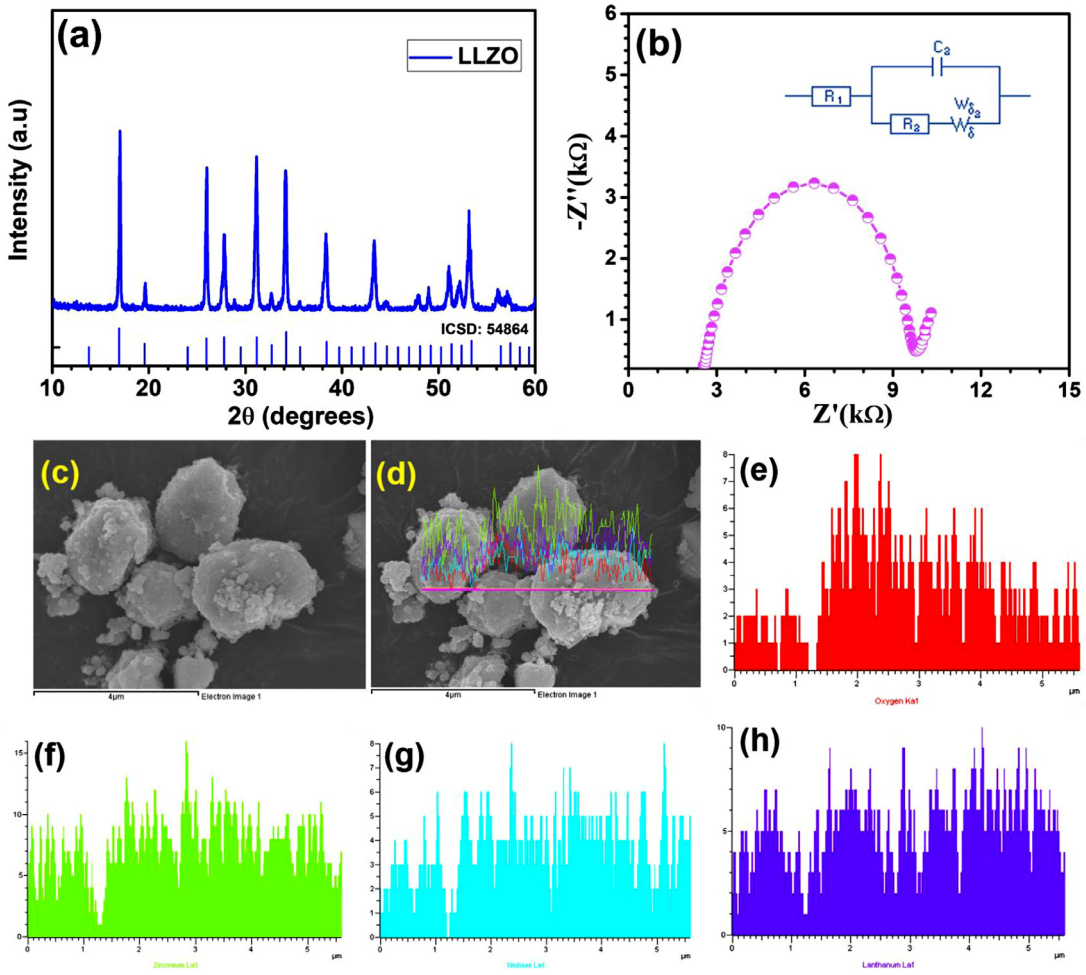

Fig. 2. (a) XRD pattern, (b) EIS curve for the prepared LLZO along with the equivalent circuit, (c) SEM image, (d) EDS mapping image for (e-h) oxygen, zirconium, niobium, and lanthanum elements in the prepared LLZO. (For interpretation of the references to colour in this figure legend, the reader is referred to the web version of this article.)

3. Results and discussion

3.1. Physical characterization

The XRD was used to analyze the structure and phase analysis of the LLZO electrolyte. The XRD pattern obtained for the Nb-LLZO material is shown in Fig 2a. The high-intensity reflections indicate the formation of a cubic phase (space group=Ia-3d) without any secondary tetragonal phase (space group=I_{41}/acd) as an impurity [8,34]. The observed high-intensity peaks positioned at 17.05°, 26.01°, 31°, and 34.20° correspond to the (112), (123), (042), and (224) planes, respectively, and reveal the formation of the LLZO solid electrolyte. The obtained high-intensity crystalline peaks are consistent with the parent $Li_5La_3Nb_2O_{12}$ structure (ICSD: 54,864). [35] The calculated lattice parameter value reveals the formation of a cubic structure with a lattice constant of 12.89 Å. [36] The crystallite size of the LLZO was estimated to be 23–47 nm using the Debye-Scherrer formula. [37] The impedance and ionic conductivity of the Li-ion conductor were calculated using the *ac* impedance spectra. The Cole-Cole plot of the prepared LLZO impedance spectra is shown in Fig. 2b. For EIS measurements, both sides of the pellet surfaces were sputtered with a layer of Pt. The EIS spectra show a semicircle at high and medium frequencies and a nearly vertical line in the low-frequency region. The semicircle represents the bulk, and the grain boundary resistance (total) of the electrolyte and the vertical line may be due to the Li-ion trans-

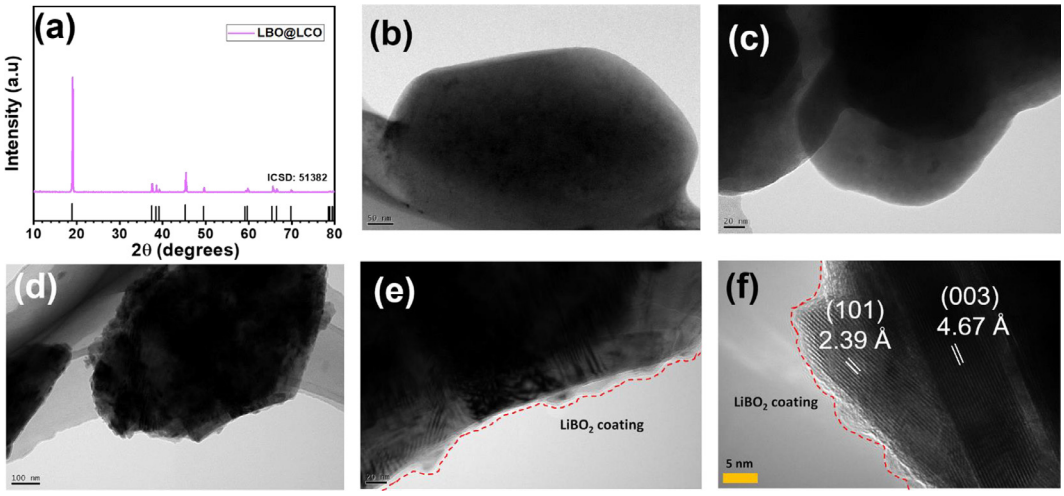

Fig. 3. (a) XRD pattern of LBO@LCO, (b, c) TEM image of bare LCO particles, (d, e) TEM image and (f) HR-TEM image of LBO@LCO particles.

fer resistance between the electrolyte and electrode. [38] The total ionic conductivity, σ_{total}, of the prepared LLZO was estimated to be 1.3×10^{-5} S cm^{-1} at ambient temperature from the EIS measurement. This was employed as the solid electrolyte towards the fabrication of the ASSLIB. The observed ionic conductivity is slightly inferior to the literature data (in the order of 10^{-4} S cm^{-1}) which is mainly due to its crystal structure and its relative density. Specifically, our solid electrolyte exhibits lower relative density of ~74%. The morphology of the electrolytes was studied by FE-SEM. The FE-SEM images confirm the coarsely shaped nature of the LLZO particles (Fig. 2c). The particle size was approximately in the range of 2–4 µm. The EDS mapping analysis (Fig. 2d) revealed that oxygen, zirconium, niobium, and lanthanum elements were uniformly distributed in the LLZO matrix (Fig. 2e-h).

Fig. 3a shows the XRD pattern of LBO-coated LCO powder. The collected reflections are well-matched with a hexagonal structure (R-3 m space group), and there is no appearance of impurity phases. The lattice parameter values for the LBO-coated LCO were calculated to be $a = 2.813$ Å and $c = 13.95$ Å. Figs. 3b–f show TEM images of the bare LCO and LBO-coated LCO particles. The TEM images (Figs. 3d & e) of the LBO@LCO particle show coarse surface features, where the LBO particles have encapsulated the surface of LCO particles after the high-energy ball-milling process. This has been clearly validated with the elemental mapping, and the image clearly shows the presence of Boron over the LCO particle (Fig. S1.) The HR-TEM image further confirmed that LBO is coated with a thickness of 2–3 nm on the surface of LCO particles (Fig. 3f). The corresponding *d* spacing values were (4.67 Å and 2.39 Å) calculated from the HR-TEM pictures which perfectly matches with the (003) and (101) plane places of LCO. These results suggest that the coated LBO melted at high temperature (700 °C) and was able to occupy the voids between the cathode and electrolyte particles [32,39].

Fig. 4a shows FE-SEM images of the bare LCO+LLZO, and 4b shows LBO@LCO+LLZO composites, respectively. The FE-SEM image (Fig. 4a) of the bare LCO composite shows a slight aggregation of the particles, which leads to poor contact between the cathode and electrolyte. In contrast, over the pristine composite, LBO was melted and encapsulated over the cathode and electrolyte particles after heat treatment. [39] As expected, the coated LBO plays a crucial role in the surface contact across the cathode/electrolyte interface during the sintering (700 °C) process. Figs. 4c and d illustrate the cross-sectional FE-SEM images of the bare LCO composite/LLZO and LBO@LCO composite/LLZO electrolyte interface, respectively. The thickness of the cathode composite was approximately 10 µm. Fig. 4c shows the cross-sectional FE-SEM image of bare LCO-LLZO composite after heat treatment, which is composed of voids in the interface, reflecting the poor interfacial contact between the cathode composite and electrolyte. These interfacial voids normally lead to the poor electrochemical performance of the cell. The underprivileged contact interrupts the Li-ion percolation pathways, and thus hinders the overall charge-transfer kinetics at the interface. Conversely, the FE-SEM images of the LBO@LCO composite and LLZO electrolyte (Fig. 4d) show the effective and much-improved contact between them without forming any interfacial voids. At 700 °C, the coated LBO became a eutectic phase and occupied the voids between the cathode and electrolyte interface. [39] Therefore, the surface modification of LBO dramatically reduces the interfacial resistance, thereby increasing Li-ion transport.

3.3. Electrochemical performance of ASSLIB

Electrochemical impedance spectroscopy (EIS) is a convenient tool to study interfacial properties, especially at the interface. In the present case, the EIS has primarily been used to measure the charge transfer resistance, R_{ct}. [38] Fig. 5a presents the Nyquist plot of the surface-modified and unmodified cathodes in ASSLIB configuration. The R_{ct} value of the unmodified cell shows a value of 7.52 kΩ, whereas the LBO-modified LCO has a value of only 3.14 kΩ because of the favorable contact between the electrode and electrolyte interface. Fig. 5b shows the comparative CV of unmodified and modified LCO composites in ASSLIB configuration. To obtain a suitable charge/discharge process, LCO should contain the electronic and ionic conductive networks that enable electron and Li-ion transport in the cathode. The LLZO powder was added to the LCO cathode so that the LLZO electrolyte can act as a Li-ion conductor; however, the non-modified battery has low capacity because of intermittent Li-ion conductive network. The redox peak confirms that the charge/discharge process in the battery is due to the Li-ion de-intercalation/ intercalation process in the cathode [29,40] (inset Fig. 5b). The peak intensity is low for the unmodified LCO, which is attributed to the poor contact between the cathode composite and electrolyte interface (Fig. 5b). The LBO- modified LCO displayed a prominent oxidation peak at ~4.28 V *vs.* Li with a high current response compared to the unmodified LCO electrode which clearly indicates the Li-extraction from the LCO cathode upon charge process. A reduction peak at ~3.75 V *vs.* Li appeared because of the intercalation of Li ions during the discharge process [27] (Fig 5b). Therefore, it is obvious that the solid-state

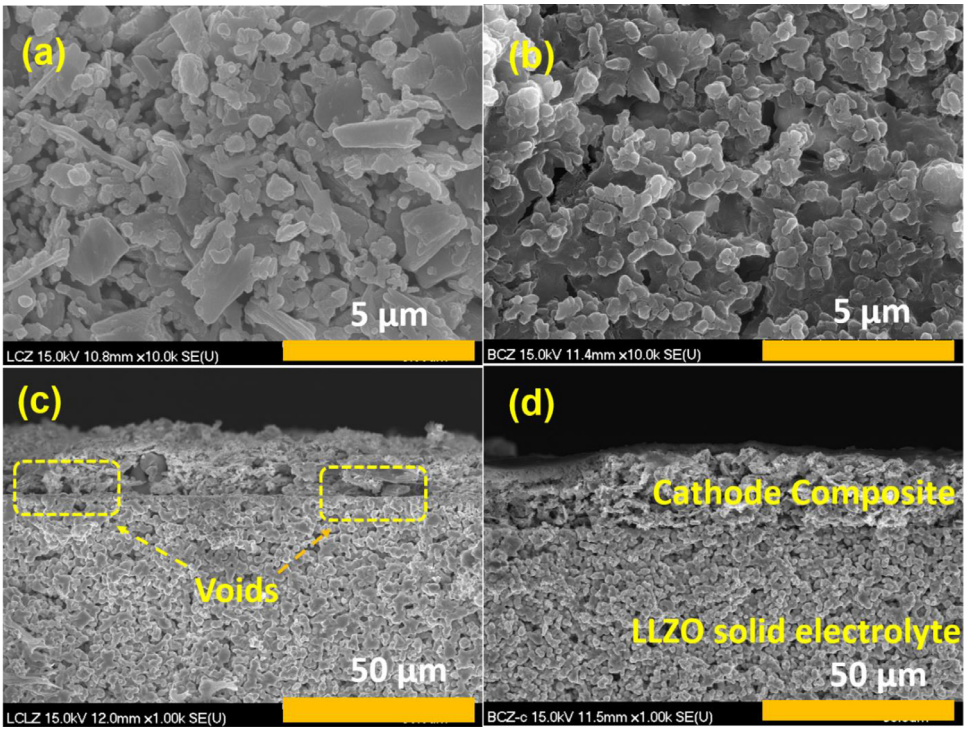

Fig. 4. Top surface and cross-sectional interface of the (a, c) LCO/LLZO composite and (b, d) LBO@LCO/LLZO composite after 700 °C heat treatment.

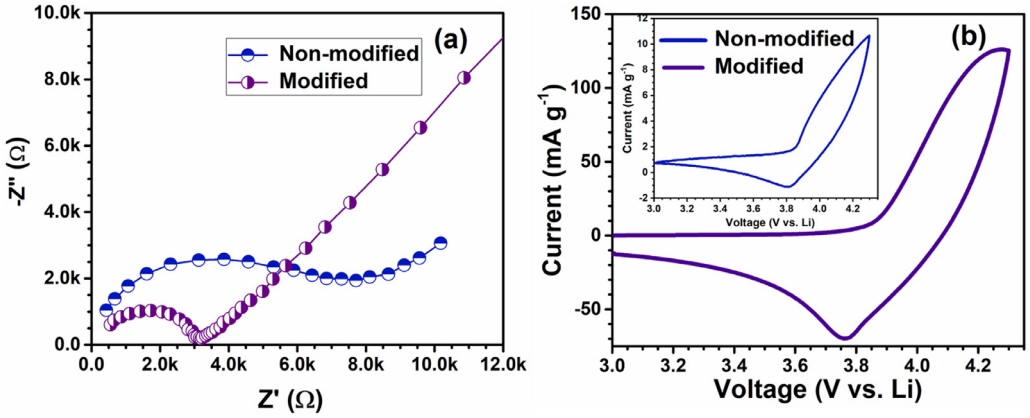

Fig. 5. Comparison of unmodified and modified cathode solid-state battery. (a) EIS curve, (b) CV curve at a scan rate of 0.1 mV s^{-1}. The electrochemical performance of the cell was tested at 80 °C.

battery has a suitable connection between the LCO cathode and Li metal anode as a result of the LBO modification.

The electrochemical performance of the ASSLIB was studied to extract 0.5 mol Li; hence, the potential window was adjusted between 3 and 4.3 V *vs.* Li. The charge/discharge studies were performed at a rate of 0.1 C. For a comparison of the electrochemical performance, and we provide a liquid cell test in the supporting information (Figure S2). The inset image of Fig. 6a confirms that there is no prominent voltage plateau in the unmodified cell, which can be attributed to the poor adhesion between the electrode and electrolyte; this is in consistent with the CV studies. The cell delivered initial capacities of 8 and 4 mAh g^{-1} for charge and discharge, respectively, with a Coulombic efficiency of ~50%. Upon prolonged cycling, there is no marked improvement in the charge and discharge performance of the unmodified cell. For the LBO-modified LCO, a discharge capacity of ~120 mAh g^{-1} was observed, which is better not only than that of the unmodified LCO but also than those of previously reported works on similar configurations listed in Table T1 [48–50]. Initially, the cells rendered a Coulombic efficiency of only ~77%; however, after three cycles, the efficiency of the cell approached >97% because of the formation of a stable interface layer (Fig. 6b, c)[41,42]. Although excellent reversibility is observed for the LBO-modified LCO-based ASSLIB, the capacity tends to decrease upon cycling; for example, after 40 cycles, the cell displayed capacity of 60 mAh g^{-1}. This corresponds to a capacity retention of 50%. In this potential range, the continuous formation of the inactive phase between the LCO and LLZO across the interfacial region, which leads to the decline in the capacity profile upon extended cycling [30,43,44].

To suppress the undesirable side reaction with LCO and LLZO, we altered the potential window from 4.3 to 4.1 V *vs.* Li. Fig. 7 shows the electrochemical performance of the LBO-modified LCO-based ASSLIB. After adjusting the cut-off voltage (3–4.1 V *vs.* Li), the cell displayed capacities of 121 and 101 mAh g^{-1} for the first charge and discharge, respectively, with a Coulombic efficiency of ~83% (Fig. 7a, b). After the 1st cycle, the Coulombic efficiency of

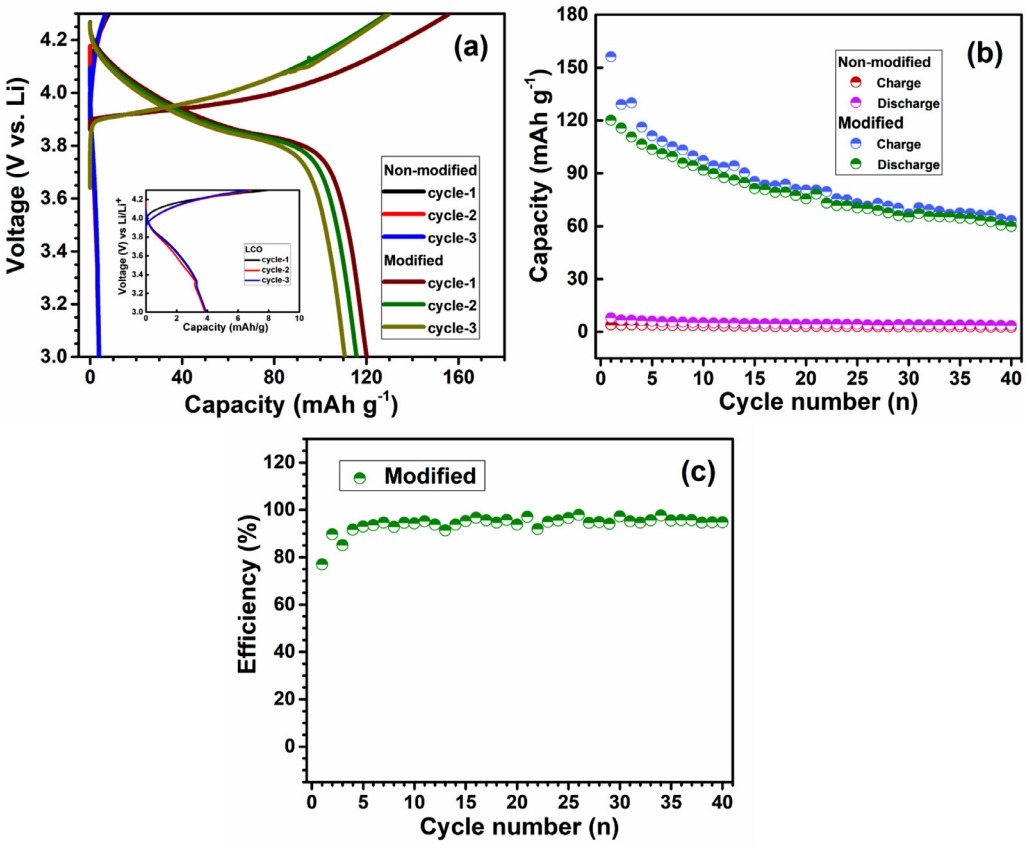

Fig. 6. Comparison of non-modified and modified cathode solid-state batteries. (a) Charge/discharge for the first three cycles, (b) cycle life of the non-modified cell at a current density of 3 μA/cm^2. (c) Efficiency curve of the modified cathode solid-state battery. The electrochemical performance of the cell was tested at 80 °C.

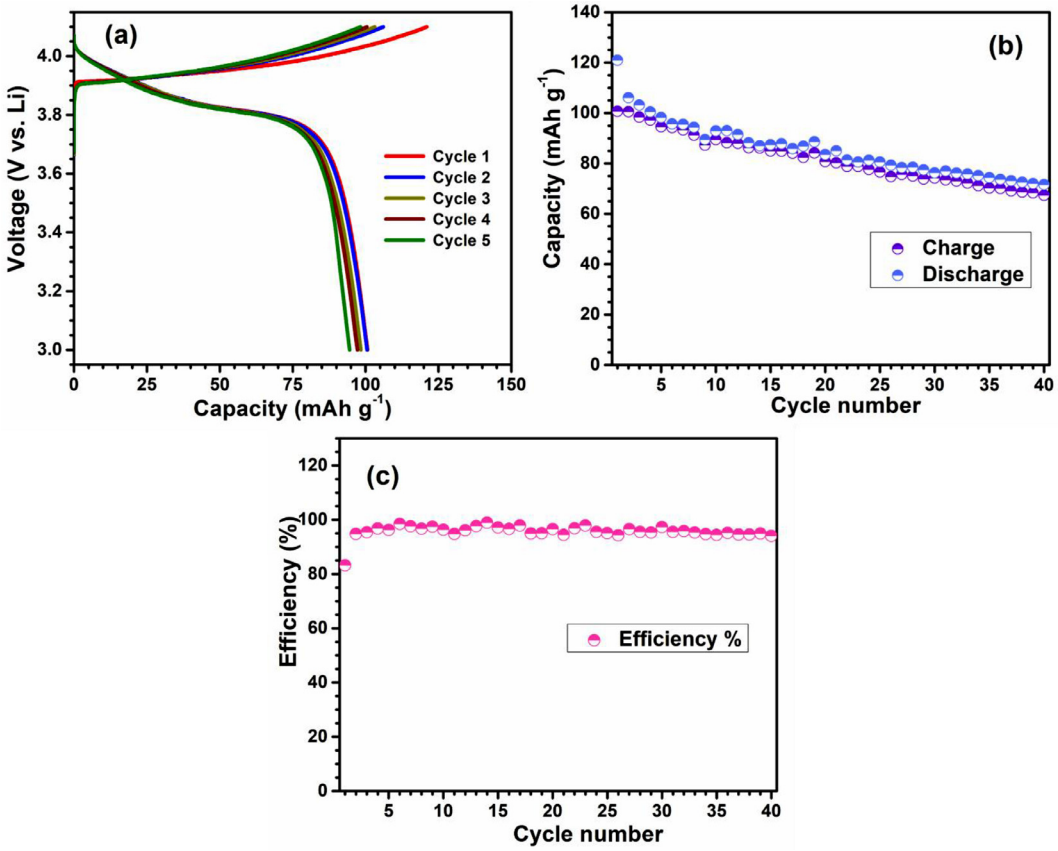

Fig. 7. Modified cathode solid state battery working potential in the range of 3–4.1 V *vs.* Li. (a) The charge-discharge curve for the first five cycles, (b) cycle life of the cell at a rate of 0.1 C. (c) Efficiency curve of the cell. The electrochemical performance of the cell was tested at 80 °C.

the cell tends to >99% because of the much-improved interfacial electrode-electrolyte contact enabled by the LBO encapsulation. After 40 cycles, the cell retained a discharge capacity of 67 mAh g^{-1} with a capacity retention of ~66% (Fig. 7b, c). During the electrochemical process, the capacity loss primarily occurred as a result of the mechanical degradation of the cathode/electrolyte interface. [45] To further understand the degradation process of the cell, we are currently pursuing *in-situ* and post mortem analyses of the ASSLIB.

The enhanced electrochemical activity was observed for the LBO@LCO composite compared with the unmodified LCO. This enhanced performance occurred mostly because of the formation of the LBO eutectic phase at a high temperature (700 °C), which efficiently binds the LCO and LLZO particles [32,39]. Based on this study, we believe that the high-voltage stable coating layer over the active material-based cathode composite should further improve the electrochemical performance in terms of capacity, cycle life, and rate capability [46,47]. Accordingly, further research activities should proceed toward fabricating a high-performance ASSLIB configuration.

Conclusion

We successfully fabricated and demonstrated the elevated temperature (80 °C) operation of an LCO-LLZO composite-based all-solid-state Li-ion battery (ASSLIB). Achieving high capacity and cycle life for the battery necessitates interfacial modification to prevent internal resistance during the electrochemical performance. Herein, we employed an LBO coating over LCO cathode particles to enhance the interfacial contact, ionic conductivity, and mechanical stability, and to fabricate a high-performance ASSLIB with high discharge capacity (120 mAh g^{-1}). By limiting the upper cut-off potential to 4.1 V *vs.* Li, the cell translates better capacity profiles with a decent discharge capacity (101 mAh g^{-1}) and cyclability. These results illustrate that LBO encapsulation over LCO is a promising strategy to realize a garnet LLZO-based all-solid-state battery.

Authors' contributions

Balasubramaniam Ramkumar: Conceptualization, Data curation, Investigation, Visualization, Writing - original draft, Writing - review & editing. **Kim So-young:** Conceptualization, Data curation, Investigation. **Nam Chan-woo:** Conceptualization, Data curation, Investigation. **Vanchiappan Aravindan:** Data curation, Writing - review & editing. **Lee Yun-Sung:** Conceptualization, Supervision, Writing - review & editing.

Declaration of Competing Interest

The authors declare that they have no known competing financial interests or personal relationships that could have appeared to influence the work reported in this paper.

Acknowledgments

The authors gratefully acknowledge the financial support from the Ministry of Trade, Industry & Energy, Republic of Korea (10080314). VA acknowledges financial support from the Science & Engineering Research Board (SERB), a statutory body of the DST, Govt. of India, through the Ramanujan Fellowship (SB/S2/RJN-088/2016).

Supplementary materials

Supplementary material associated with this article can be found, in the online version, at doi:10.1016/j.electacta.2020.136955.

References

[1] S.A. Pervez, M.A. Cambaz, V. Thangadurai, M. Fichtner, Interface in solid-state lithium battery: challenges, progress, and outlook, ACS Appl. Mater. Interfaces 11 (2019) 22029–22050, doi:10.1021/acsami.9b02675.
[2] Y. Xiao, Y. Wang, S.H. Bo, J.C. Kim, L.J. Miara, G. Ceder, Understanding interface stability in solid-state batteries, Nat. Rev. Mater. 5 (2020) 105–126, doi:10.1038/s41578-019-0157-5.
[3] Z. Zhang, Y. Shao, B. Lotsch, Y.S. Hu, H. Li, J. Janek, L.F. Nazar, C.W. Nan, J. Maier, M. Armand, L. Chen, New horizons for inorganic solid-state ion conductors, Energy Environ. Sci. 11 (2018) 1945–1976, doi:10.1039/c8ee01053f.
[4] G.Y. Adachi, N. Imanaka, S. Tamura, Ionic conducting lanthanide oxides, Chem. Rev. 102 (2002) 2405–2429, doi:10.1021/cr0103064.
[5] H.J. Choi, S.Y. Kim, M.K. Gong, H.V. Ramasamy, V. Aravindan, Y.G. Lee, Y.S. Lee, Tailored perovskite $Li_{0.33}La_{0.56}TiO_3$ via an adipic acid-assisted solution process: a promising solid electrolyte for lithium batteries, J. Alloys Compd. 729 (2017) 338–343, doi:10.1016/j.jallcom.2017.09.160.
[6] K. Arbi, S. Mandal, J.M. Rojo, J. Sanz, Dependence of ionic conductivity on composition of fast ionic conductors $Li_{1+x}Ti_{2-x}Al_x(PO_4)_3$, $0 \leq x \leq 0.7$. A parallel NMR and electric impedance study, Chem. Mater. 14 (2002) 1091–1097, doi:10.1021/cm010528i.
[7] V. Thangadurai, H. Kaack, W.J.F. Weppner, Novel fast lithium ion conduction in garnet-type $Li_5La_3M_2O_{12}$ (M = Nb, Ta), J. Am. Ceram. Soc. 86 (2003) 437–440 doi:10.1111/j.1151-2916. 2003.tb03318.x.
[8] R. Murugan, V. Thangadurai, W. Weppner, Fast lithium ion conduction in garnet-type $Li_7La_3Zr_2O_{12}$, Angew. Chemie - Int. Ed. 46 (2007) 7778–7781, doi:10.1002/anie.200701144.
[9] H.Y.P. Hong, Crystal structure and ionic conductivity of $Li_{14}Zn(GeO_4)_4$ and other new Li+ superionic conductors, Mater. Res. Bull. 13 (1978) 117–124, doi:10.1016/0025-5408(78)90075-2.
[10] N. Kamaya, K. Homma, Y. Yamakawa, M. Hirayama, R. Kanno, M. Yonemura, T. Kamiyama, Y. Kato, S. Hama, K. Kawamoto, A. Mitsui, A lithium superionic conductor, Nat. Mater. 10 (2011) 682–686, doi:10.1038/nmat3066.
[11] S. Amaresh, K. Karthikeyan, K.J. Kim, Y.G. Lee, Y.S. Lee, Aluminum based sulfide solid lithium ionic conductors for all solid-state batteries, Nanoscale 6 (2014) 6661–6667, doi:10.1039/c4nr00804a.
[12] Y. Zhao, L.L. Daemen, Superionic conductivity in lithium-rich anti-perovskites, J. Am. Chem. Soc. 134 (2012) 15042–15047, doi:10.1021/ja305709z.
[13] H.J. Deiseroth, S.T. Kong, H. Eckert, J. Vannahme, C. Reiner, T. Zaiß, M. Schlosser, LiPSX: a class of crystalline Li-rich solids with an unusually high Li+ mobility, Angew. Chemie - Int. Ed. 47 (2008) 755–758, doi:10.1002/anie.200703900.
[14] Y. Zhu, X. He, Y. Mo, Origin of outstanding stability in the lithium solid electrolyte materials: insights from thermodynamic analyses based on first-principles calculations, ACS Appl. Mater. Interfaces 7 (2015) 23685–23693, doi:10.1021/acsami.5b07517.
[15] Y. Meesala, A. Jena, H. Chang, R.S. Liu, Recent advancements in Li-ion conductors for all-solid-state Li-ion batteries, ACS Energy Lett. 2 (2017) 2734–2751, doi:10.1021/acsenergylett.7b00849.
[16] A. Manthiram, X. Yu, S. Wang, Lithium battery chemistries enabled by solid-state electrolytes, Nat. Rev. Mater. 2 (2017) 16103 1-16, doi:10.1038/natrevmats.2016.103.
[17] X. Yan, Z. Li, Z. Wen, W. Han, $Li/Li_7La_3Zr_2O_{12}/LiFePO_4$ all-solid-state battery with ultrathin nanoscale solid electrolyte, J. Phys. Chem. C 121 (2017) 1431–1435, doi:10.1021/acs.jpcc.6b10268.
[18] B. Liu, K. Fu, Y. Gong, C. Yang, Y. Yao, Y. Wang, C. Wang, Y. Kuang, G. Pastel, H. Xie, E. Wachsman, L. Hu, Rapid thermal annealing of cathode-garnet interface toward High-Temperature solid state batteries, Nano Lett. 17 (2017) 4917–4923, doi:10.1021/acs.nanolett.7b01934.
[19] K. Takada, Interfacial nano architectonics for solid-state lithium batteries, Langmuir 29 (2013) 7538–7541, doi:10.1021/la3045253.
[20] J. Maier, Nanoionics: ionic charge carriers in small systems, Phys. Chem. Chem. Phys. 11 (2009) 3010–3022, doi:10.1039/b905911n.
[21] J. Haruyama, S. Keitaro, H. Liyuan, T. Kazunori, T. Yoshitaka, Space−charge layer effect at interface between oxide cathode and sulfide electrolyte in all-solid-state lithium-ion battery, Chem.Mater. (2014) 4248–4255.
[22] N. Ohta, K. Takada, I. Sakaguchi, L. Zhang, R. Ma, K. Fukuda, M. Osada, T. Sasaki, $LiNbO_3$-coated $LiCoO_2$ as cathode material for all solid-state lithium secondary batteries, Electrochem. Commun. 9 (2007) 1486–1490, doi:10.1016/j.elecom.2007.02.008.
[23] Y. Seino, T. Ota, K. Takada, High rate capabilities of all-solid-state lithium secondary batteries using $Li_4Ti_5O_{12}$-coated $LiNi_{0.8}Co_{0.15}Al_{0.05}O_2$ and a sulfide-based solid electrolyte, J. Power Sources 196 (2011) 6488–6492, doi:10.1016/j.jpowsour.2011.03.090.
[24] Y. Ito, Y. Sakurai, S. Yubuchi, A. Sakuda, A. Hayashi, M. Tatsumisago, Application of $LiCoO_2$ particles coated with lithium ortho-oxosalt thin films to sulfide-type all-solid-state lithium batteries, J. Electrochem. Soc. 162 (2015) A1610–A1616, doi:10.1149/2.0771508jes.
[25] Y. Ren, T. Liu, Y. Shen, Y. Lin, C.W. Nan, Garnet-type oxide electrolyte with novel porous-dense bilayer configuration for rechargeable all-solid-state lithium batteries, Ionics (Kiel) 23 (2017) 2521–2527, doi:10.1007/s11581-017-2224-5.
[26] M. Kotobuki, K. Kanamura, Y. Sato, T. Yoshida, Fabrication of all-solid-state lithium battery with lithium metal anode using Al_2O_3-added $Li_7La_3Zr_2O_{12}$ solid electrolyte, J. Power Sources 196 (2011) 7750–7754, doi:10.1016/j.jpowsour.2011.04.047.

[27] M. Kotobuki, K. Kanamura, Fabrication of all-solid-state battery using $Li_5La_3Ta_2O_{12}$ ceramic electrolyte, Ceram. Int. 39 (2013) 6481–6487, doi:10.1016/j.ceramint.2013.01.079.
[28] T. Liu, Y. Zhang, X. Zhang, L. Wang, S.X. Zhao, Y.H. Lin, Y. Shen, J. Luo, L. Li, C.W. Nan, Enhanced electrochemical performance of bulk type oxide ceramic lithium batteries enabled by interface modification, J. Mater. Chem. A 6 (2018) 4649–4657, doi:10.1039/c7ta06833f.
[29] Y. Zhang, F. Chen, D. Yang, W. Zha, J. Li, Q. Shen, X. Zhang, L. Zhang, High capacity all-solid-state lithium battery using cathodes with three-dimensional Li+ conductive network, J. Electrochem. Soc. 164 (2017) A1695–A1702, doi:10.1149/2.1501707jes.
[30] K. Park, B.C. Yu, J.W. Jung, Y. Li, W. Zhou, H. Gao, S. Son, J.B. Goodenough, Electrochemical nature of the cathode interface for a solid-state lithium-ion battery: interface between $LiCoO_2$ and garnet-$Li_7La_3Zr_2O_{12}$, Chem. Mater. 28 (2016) 8051–8059, doi:10.1021/acs.chemmater.6b03870.
[31] T. Liu, Y. Ren, Y. Shen, S.X. Zhao, Y. Lin, C.W. Nan, Achieving high capacity in bulk-type solid-state lithium ion battery based on $Li_{6.75}La_3Zr_{1.75}Ta_{0.25}O_{12}$ electrolyte: interfacial resistance, J. Power Sources 324 (2016) 349–357, doi:10.1016/j.jpowsour.2016.05.111.
[32] S. Ohta, S. Komagata, J. Seki, T. Saeki, S. Morishita, T. Asaoka, All-solid-state lithium ion battery using garnet-type oxide and Li_3BO_3 solid electrolytes fabricated by screen-printing, J. Power Sources 238 (2013) 53–56, doi:10.1016/j.jpowsour.2013.02.073.
[33] Y. Gu, J.F. Federici, Fabrication of a flexible current collector for lithium ion batteries by inkjet printing, Batteries 4 (2018) 42 1-11, doi:10.3390/batteries4030042.
[34] W. Gu, M. Ezbiri, R.P. Rao, M. Avdeev, S. Adams, Effects of penta-and trivalent dopants on structure and conductivity of $Li_7La_3Zr_2O_{12}$, Solid State Ionics 274 (2015) 100–105, doi:10.1016/j.ssi.2015.03.019.
[35] V. Thangadurai, S. Adams, W. Weppner, Crystal structure revision and identification of Li+-ion migration pathways in the garnet-like $Li_5La_3M_2O_{12}$ (M = Nb, Ta) oxides, Chem. Mater. 16 (2004) 2998–3006, doi:10.1021/cm031176d.
[36] M. Paul, Microwave assisted reactive sintering for Al doped $Li_7La_3Zr_2O_{12}$ lithium ion solid state electrolyte, Mater. Res. Exp. 6 (2016) 1–27.
[37] S.A. Yoon, N.R. Oh, A.R. Yoo, H.G. Lee, H.C. Lee, Preparation and characterization of Ta-substituted $Li_7La_3Zr_{2-x}O_{12}$ garnet solid electrolyte by sol-gel processing, J. Korean Ceram. Soc. 54 (2017) 278–284.
[38] J.F. Wu, W.K. Pang, V.K. Peterson, L. Wei, X. Guo, Garnet-type fast Li-ion conductors with high ionic conductivities for all-solid-state batteries, ACS Appl. Mater. Interfaces 9 (2017) 12461–12468, doi:10.1021/acsami.7b00614.
[39] N.C. Rosero-Navarro, T. Yamashita, A. Miura, M. Higuchi, K. Tadanaga, Preparation of $Li_7La_3(Zr_{2-x},Nb_x)O_{12}$ (x = 0-1.5) and $Li_3BO_3/LiBO_2$ composites at low temperatures using a sol-gel process, Solid State Ionics 285 (2016) 6–12, doi:10.1016/j.ssi.2015.06.015.
[40] T. Kato, T. Hamanaka, K. Yamamoto, T. Hirayama, F. Sagane, M. Motoyama, Y. Iriyama, In-situ $Li_7La_3Zr_2O_{12}/LiCoO_2$ interface modification for advanced all-solid-state battery, J Power Sources 260 (2014) 292–298, doi:10.1016/j.jpowsour.2014.02.102.
[41] C.L. Tsai, Q. Ma, C. Dellen, S. Lobe, F. Vondahlen, A. Windm¨uller, D. Gr¨uner, H. Zheng, S. Uhlenbruck, M. Finsterbusch, F. Tietz, D. Fattakhova-Rohlfing, H.P. Buchkremer, O. Guillon, A garnet structure-based all-solid-state Li battery without interface modification: resolving incompatibility issues on positive electrodes, Sustain Energy Fuels 3 (2019) 280–291, doi:10.1039/c8se00436f.
[42] K. Nie, Y. Hong, J. Qiu, Q. Li, X. Yu, H. Li, L. Chen, Interfaces between cathode and electrolyte in solid state lithium batteries: challenges and perspectives, Front. Chem. 616 (6) (2018) 1–19 doi.org/10.3389/fchem.2018.00616.
[43] L.J. Miara, William D Richards, Y.E. Wang, G. Ceder, First-principles studies on cation dopants and electrolyte|cathode interphases for lithium garnets, Chem. Mater 27 (2015) 4040–4047, doi:10.1021/acs.chemmater.5b01023.
[44] Y. Zhu, X. He, Y. Mo, First principles study on electrochemical and chemical stability of solid electrolyte–electrode interfaces in all-solid-state Li-ion batteries, J. Mater. Chem. A 4 (2016) 3253–3266, doi:10.1039/c5ta08574h.
[45] F. Han, J. Yue, C. Chen, N. Zhao, X. Fan, Z. Ma, T. Gao, F. Wang, X. Guo, C. Wang, Interphase engineering enabled all-ceramic lithium battery, Joule 2 (2018) 497–508, doi:10.1016/j.joule.2018.02.007.
[46] Y. Xiao Y, L.J. Miara, Y. Wang, G. Ceder, Computational screening of cathode coatings for solid-state batteries, Joule 3 (2019) 1252–1275, doi:10.1016/j.joule.2019.02.006.
[47] C. Yu, S. Ganapathy, E.V. Eck, H. Wang, S. Basak, Z. Li, M. Wagemaker, Accessing the bottleneck in all-solid-state batteries, lithium-ion transport over the solid-electrolyte-electrode interface, Nat. Commun. 8 (2017) 1–9, doi:10.1038/s41467-017-01187-y.
[48] S. Ohta, T. Kobayashi, J. Seki, T. Asaoka, Electrochemical performance of an all-solid-state lithium ion battery with garnet-type oxide electrolyte, J. Power Sources 202 (2012) 332–335, doi:10.1016/j.jpowsour.2011.10.064.
[49] S. Ohta, J. Seki, Y. Yagi, T.Tani Y.Kihira, T. Asaoka, Co-sinterable lithium garnet-type oxide electrolyte with cathode for all-solid-state lithium ion battery, J. Power Sources. 265 (2014) 40–44, doi:10.1016/j.jpowsour.2014.04.065.
[50] G.V. Alexander, N.C. Rosero-Navarro, A. Miura, K. Tadanaga, R. Murugan, Electrochemical performance of a garnet solid electrolyte-based lithium metal battery with interface modification, J. Mater. Chem. A 6 (2018) 21018–21028, doi:10.1039/C8TA07652A.